Analytical Methods

Accepted Manuscript

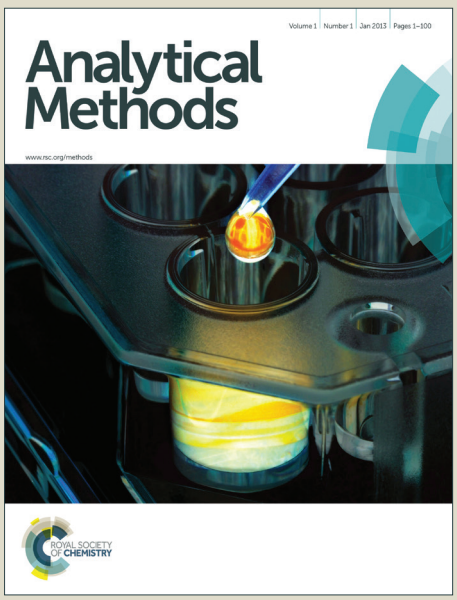

ROYAL SOCIETY OF CHEMISTRY

www.rsc.org/methods

Cite this: DOI: 10.1039/c0xx00000x

www.rsc.org/xxxxxx

ARTICLE TYPE

Fluorescence resonance energy transfer-based aptamer biosensor for bisphenol A using lanthanide-doped $KGdF_4$ nanoparticles

Nuo Duan,[a] Hui Zhang,[b] Yu Nie,[a] Shijia Wu,[a] Tingting Miao,[c] Jie Chen[a] and Zhouping Wang*[a]

Received (in XXX, XXX) Xth XXXXXXXXX 20XX, Accepted Xth XXXXXXXXX 20XX

DOI: 10.1039/b000000x

We report a method for trace detection of bisphenol A (BPA) based on fluorescence resonance energy transfer (FRET) between lanthanide-doped $KGdF_4$ nanoparticles ($KGdF_4$:Tb^{3+} NPs) as a donor, and gold nanoparticles (AuNPs) that acts as an acceptor. The $KGdF_4$:Tb^{3+} NPs were modified with an aptamer recognizing BPA, and AuNPs were modified with the complementary DNA (cDNA) of the aptamer. The donor-acceptor pair was fabricated by hybridizing the aptamers and their cDNA. Thus, fluorescence of the $KGdF_4$:Tb^{3+} NPs could be quenched due to good overlap between the $KGdF_4$:Tb^{3+} NPs fluorescence emission and the AuNPs absorption spectrum. However, on addition of BPA, the aptamers preferentially bound to BPA, forming $KGdF_4$:Tb^{3+} NPs-aptamer-BPA complexs. As a result, the FRET was disrupted, and the fluorescence was restored. The recovered fluorescence of the $KGdF_4$:Tb^{3+} NPs was linearly proportional to the concentration of BPA in the range of 0.5 to 100 ng·mL^{-1}, with detection limits as low as 0.16 ng·mL^{-1}. The assay was applied to real samples, and the results were consistent with the results obtained using high performance liquid chromatography (HPLC) methods. We presume that this strategy can be extended to the detection of other contaminants by simply substituting the aptamer.

Introduction

Bisphenol A (BPA, 4,4'-isopropylidenediphenol), is an important chemical used principally as a monomer in manufacturing a multitude of chemical products that include epoxy resins and polycarbonate [1,2]. Among other uses, these manufactured materials are extensively used as food containers (e.g., milk, water, and infant bottles) and food can linings [3-5]. Heat and either acidic or basic conditions accelerate the hydrolysis of the ester bond linking BPA monomers, leading to BPA release and migration into the food, which produces negative effects on human health. BPA is postulated to cause reproductive disorders, such as sperm count decline; birth defects due to fetal exposure; and various types of cancers (e.g., prostate, testicular, and breast cancer) and has diverse pleiotropic actions in the brain and cardiovascular system [6-8]. Therefore, considerable attention has been devoted to the determination of BPA.

Currently, many analytical methods have been developed for sensing BPA. The detection techniques most frequently used for BPA are liquid chromatography-mass spectrometry (LC-MS) [9,10] and gas chromatography-mass spectrometry (GC-MS) [11,12]. These strategies are highly sensitive and specific, but require time-consuming pre-treatment steps, and the instruments required are rather complicated and expensive and are therefore rarely employed for on-site measurements. Recently, different types of bioassays for sensing BPA have been developed, such as immunochemical [13,14] and electrochemical assays [15,16]. However, these immunobioassays are heavily reliant on the quality of the antibodies used. The preparation of the antibodies via animal immunization is time-consuming (several months), and the antibody may become susceptible to stability or modification issues.

To overcome the above limitations, alternatives to antibody based biosensors for analytical applications are an area of active research. Aptamers are single-stranded nucleic acid molecules that are derived from random, single-stranded nucleic acid sequence pools and can be selected via a process termed SELEX (Systematic Evolution of Ligands by Exponential Enrichment) [17,18]. These selected aptamers can bind a wide range of targets, ranging from small molecules [19] to proteins [20] as well as whole cells [21] with high affinity and specificity. Owing to their high selectivity, stability, versatile target binding, and easy regeneration capabilities compared with antibodies, aptamers have received considerable attention as recognition probes in bioassays [22,23].

FRET is widely used as a reliable analytic strategy in biological analyses [24] due to its strong merits, such as its high sensitivity, noninvasiveness, and homogeneous assay performance. FRET is a nonradioactive process, in which energy transfers from a luminescent donor to an acceptor via a dipole-dipole interaction over a short distance (1-10 nm) [25]. The use of appropriate donor-acceptor pairs is extremely critical for improving the efficiency of the FRET and the resulting analytical performance.

Recently, the fluoride host materials with composition $MGdF_4$ (M= Li, Na, or K) are of particular interest. Due to its structural and optical properties, the Ln^{3+} (Tb^{3+}, Eu^{3+}…) doped $KGdF_4$ nanoparticles have received more and more attention. Compared with conventional organic dyes and quantum dots, Ln^{3+} doped

$KGdF_4$ possessing superior features, including long luminescence lifetime (microsecond-millisecond range), large Stokes shift (>50 nm), narrow emission bandwidths (<10 nm), low toxicity, and high luminescence quantum yields and high resistance to photobleaching. Thus, it has been suggested as a promising new class of fluorescent probes.

Herein, we demonstrate the use of $KGdF_4:Tb^{3+}$ NPs as an energy donor and AuNPs, with high energy absorption efficiency, as an energy acceptor to develop a FRET system that can be employed for quantitative detection of BPA. The strong fluorescence of $KGdF_4:Tb^{3+}$ NPs, the high affinity and specificity of aptamers and the unique FRET between $KGdF_4:Tb^{3+}$ NPs and AuNPs were utilized in quantitative analyses of BPA. Moreover, the sensor design is general and can be applied to other aptamer-based sensors. Our developed quenching mechanism and obtained results should be of special interest for biosensing applications.

Materials and methods

Reagents and apparatus

$TbCl_3 \cdot 6H_2O$ and BPA were purchased from Aladdin Industrial Inc. (Shanghai, China). KCl, NH_4F, $HAuCl_4$, trisodium citrate, glutaraldehyde, and glycol were all of analytical grade. All of these chemicals were purchased from Sinopharm Chemical Reagent Co., Ltd. (Shanghai, China). $GdCl_3 \cdot 6H_2O$, polypropyleneimine (PEI), and avidin were purchased from Sigma-Aldrich (U.S.A.). BPA aptamers [26] and its complementary DNA were synthesized by the Shanghai Sangon Biological Science & Technology Company (Shanghai, China). The DNA sequence of the BPA aptamer is 5'-biotin-CCGGTGGGTGGTCAGGTGGGA**TAGCGTTCCGCGTAT**GGCCCAGCGCATCACGGGTTCGCACCA-3'. The cDNA sequence is 5'-SH-ATACGCGGAACGCTA-3', which is partly complementary to the aptamer sequence in bold.

Transmission electron microscopy (TEM) was performed with a JEOL model 2100HR instrument operating at a 200 kV accelerating voltage (TEM, JEOL Ltd., Japan). X-ray diffraction (XRD) measurements were performed using a D8-Advance diffractometer (Bruker AXS Ltd., Germany). UV-visible (UV-vis) absorption spectra were measured using a UV-1800 spectrophotometer (Shimadzu Co., Japan). Fourier transform infrared (FT-IR) spectra of the bionanoparticles were obtained with a Nicolet Nexus 470 FT-IR spectrophotometer (Thermo Electron Co., U.S.A.) using the KBr method. $KGdF_4:Tb^{3+}$ fluorescence spectra were measured with a Fluormax-4 fluorescence spectrophotometer (HORIBA Co., U.S.A.).

Preparation of $KGdF_4:Tb^{3+}$ NPs

First, 2.0 mmol KCl, 1.0 mmol $GdCl_3 \cdot 6H_2O$ powder and 1 mL (300 $mg \cdot mL^{-1}$) PEI were added to 20 mL of glycol in a flask. Next, 0.01 mmol $TbCl_3 \cdot 6H_2O$ powder was added and the mixture was stirred thoroughly, forming a homogeneous solution. Next, 8 mmol NH_4F was dissolved in 20 mL of glycol, followed by agitation under 40 °C. The freshly prepared NH_4F solution mentioned above was then added dropwise to the previously prepared solution under vigorous stirring for 1 h. The colloidal solution was then transferred to a 50 mL Teflon–lined autoclave, sealed, and heated at 195 °C for 4 h. After the mixture cooled to room temperature, the products were deposited by adding ethanol to the bottom of the vessel, centrifuged to obtain a powdered sample, washed with ethanol and distilled water several times, and then dried in an oven at 60 °C.

Preparation of AuNPs

All glassware was cleaned in aqua regia (HCl/HNO_3, 3:1), rinsed with triply distilled H_2O, and then oven-dried prior to use. The AuNPs were synthesized using a common method: reducing developed gold ions with sodium citrate [27]. In this procedure, 95.8 mL of triply distilled H_2O and 4.2 mL of 1% $HAuCl_4$ were boiled with vigorous stirring for 10 min, and 10 mL of 1% trisodium citrate was rapidly added. The solution turned blue within 25 s, and a final color change to red-violet occurred 1 min later. The solution was boiled for an additional 10 min. The heating source was then removed, and the colloid suspension was stirred for another 15 min and then allowed to cool to room temperature.

Attachment of aptamers to $KGdF_4:Tb^{3+}$ NPs

Amino-modified $KGdF_4:Tb^{3+}$ NPs were conjugated with avidin using a classical glutaraldehyde method [28]. Typically, 15 mg of $KGdF_4:Tb^{3+}$ NPs was dispersed into 5 mL of 10 mM phosphate buffer solution (PBS, pH 7.4) by ultrasonication for 20 min, and then 1.25 mL of 25% glutaraldehyde was added to the mixture. The mixture was agitated slowly on a shaking table at room temperature for 2 h, and the $KGdF_4:Tb^{3+}$ NPs were separated by centrifugation and washed with PBS three times. Subsequently, the resultant $KGdF_4:Tb^{3+}$ NPs were dispersed into 0.9 mL of 10 mM PBS by ultrasonication, followed by the addition of 1.0 $mg \cdot mL^{-1}$ avidin (100 μL). The mixture was shaken slowly on a shaking table at room temperature for 12 h. The avidin-conjugated $KGdF_4:Tb^{3+}$ NPs were separated and washed with PBS three times, discarding the supernatant each time. The resulting avidin-activated $KGdF_4:Tb^{3+}$ NPs (1 $mg \cdot mL^{-1}$) and 10 μL of 5'-biotin modified aptamers (100 μM) were conjugated under gentle mixing for 12 h. Finally, aptamers were covalently attached to $KGdF_4:Tb^{3+}$ NPs through avidin-biotin specific binding, followed by blocking the nanoparticles with a 2% bovine serum albumin (BSA) solution.

Attachment of cDNA to AuNPs

The procedure for conjugating the AuNPs to cDNA was adapted from a previously reported protocol [29]. This protocol was based on the Au-S interactions that occur between the gold lattice and thiolated oligonucleotides. Briefly, 10 μL of 100 μM cDNA was added to 1 mL of AuNPs solution. After reacting for 16 h, the AuNPs-cDNA complexes were "aged" with salts (0.1 M NaCl, 10 mM phosphate, pH 7.4) for 40 h. The solution was then centrifuged at 12,000 rpm for 15 min. The supernatant was removed, and the solid at the bottom of the tube was dispersed into binding buffer (10 mM Tris–HCl, pH 8.0, 100 mM KCl, 1 mM $MgCl_2$) for subsequent experiments.

Trace detection of BPA based on FRET assays and data analyses

For trace detection of BPA, 200 μL of aptamer-functionalized $KGdF_4:Tb^{3+}$ NPs and 200 μL of cDNA functionalized AuNPs were first incubated for 1 h at 37 °C. Next, sample solutions

containing various concentrations of BPA were added to the above solution, and further incubated for 45 min at room temperature. The fluorescence signals of $KGdF_4:Tb^{3+}$ NPs were measured at 542 nm wavelengths by excitation at 273 nm. All experiments were repeated three times, and each sample solution was measured five times. Slits for both the excitation and the emission were set at 5 nm.

Results and discussion

Principle of the FRET aptamer sensor for BPA detection

Scheme 1 outlines the working principle of the aptamer biosensor based on FRET for the trace detection of BPA. First, biotin-modified aptamers were covalently attached to avidin-functionalized $KGdF_4:Tb^{3+}$ NPs, and thiol-modified cDNA of the aptamers was conjugated to the AuNPs through strong Au-S bonds formation. Then, aptamer-$KGdF_4:Tb^{3+}$ NPs were hybridized with cDNA-AuNPs to form duplex structures. This hybridization process brings energy donor $KGdF_4:Tb^{3+}$ NPs into close proximity of energy acceptor AuNPs, resulting in significant fluorescence quenching due to the energy transfer effect. In the presence of BPA, the aptamers bound to their target with high affinity and specificity, forming stable $KGdF_4:Tb^{3+}$ NPs-aptamer-target complexes. This complexation leads to changes in the formation of the aptamers and thereby induces the dehybridization of the cDNA-AuNPs. This effect became sufficiently large to prevent fluorescence quenching, and thus, the fluorescence was recovered. In this way, the observed recovered fluorescence intensity of $KGdF_4:Tb^{3+}$ NPs could be used as an indicator for BPA detection.

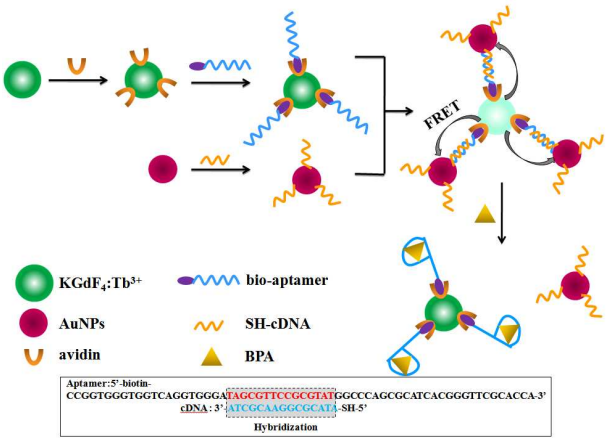

Scheme. 1 Schematic illustration of the FRET from $KGdF_4:Tb^{3+}$ NPs-aptamer to AuNPs-cDNA for the trace detection of BPA

Characterization of $KGdF_4:Tb^{3+}$ NPs and AuNPs

The amine-functionalized $KGdF_4:Tb^{3+}$ NPs applied herein were prepared with a one-pot synthesis in the presence of PEI. Fig. 1A shows representative TEM images of the $KGdF_4:Tb^{3+}$ NPs. As observed, the $KGdF_4:Tb^{3+}$ NPs are well-dispersed and uniform in size with average diameters of approximately 25±5 nm (Fig. 1B). In addition, PEI was used to modify the $KGdF_4:Tb^{3+}$ NPs with an amino group, allowing the $KGdF_4:Tb^{3+}$ NPs to be dispersed into water. The surface modifications of $KGdF_4:Tb^{3+}$ NPs were identified by FT-IR spectroscopy. As shown in Fig.1C, the strong IR bands at 1396, 2950 and 2856 cm^{-1} were attributed to the stretching vibrations of the C−N bond and asymmetric and symmetric stretching vibrations of the C−H bond, respectively. Meanwhile, a strong band centered at 1625 cm^{-1} was observed, which can be attributed to the N−H bending mode of an amino group ($-NH_2$), thereby revealing the PEI capping on the surface of the NPs. Thus, the FT-IR results indicate that the $KGdF_4:Tb^{3+}$ NPs were functionalized with amino groups in the synthetic process. Fig. 1D shows the XRD pattern of $KGdF_4:Tb^{3+}$ NPs, which can be exclusively indexed to cubic phase of $KGdF_4$ in accordance with the pure phase of $KGdF_4$ [30]. The results indicate the presence of highly crystalline $KGdF_4$ NPs without any other impurities. To examine the potential application in FRET determination, the fluorescence lifetime of Tb^{3+} doped $KGdF_4$ NPs was measured at 542 nm of its characteristic emission (Fig. 1E), with the decay time of 8.57±0.05 ms by single-exponential function. The NPs were well-reproducible in controlled synthesis conditions.

The prepared AuNPs were spherical with an average diameter of 15 nm (Fig. 1F). The absorption spectrum of AuNPs used in this work (Fig. 2a) displayed a strong absorption band at approximately 525 nm, overlapping the fluorescence spectra of $KGdF_4:Tb^{3+}$ NPs, which exhibited a significant green emission at 542 nm (Fig. 2b). Thus, FRET possibly resulted between the $KGdF_4:Tb^{3+}$ NPs (donor) and the AuNPs (acceptor).

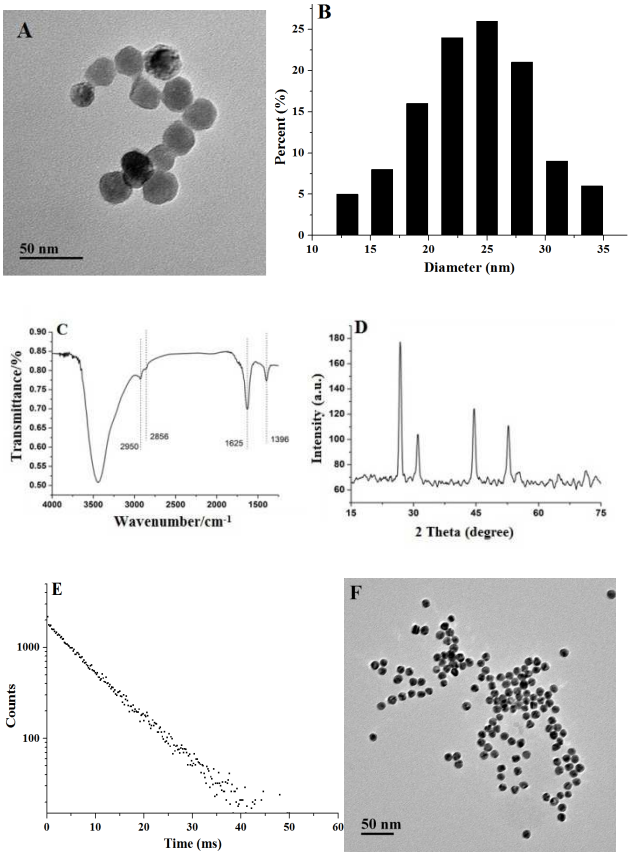

Fig.1 A TEM image (A), the size distribution (B), the FT-IR spectrum (C), the XRD pattern (D), and time-resolved fluorescence decay curve (E) of $KGdF_4:Tb^{3+}$ NPs. A TEM image of AuNPs (F)

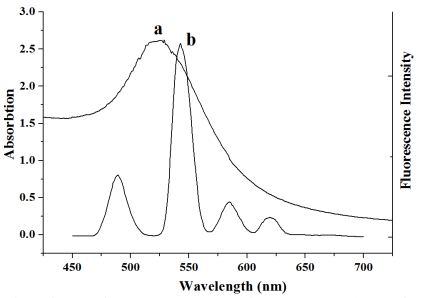

Fig. 2 UV-vis absorption spectrum of AuNPs (a) and fluorescence emission spectrum of $KGdF_4:Tb^{3+}$ NPs (b)

Characteristics of aptamer-conjugated $KGdF_4:Tb^{3+}$ NPs and cDNA-functionalized AuNPs

Aptamers were conjugated to $KGdF_4:Tb^{3+}$ NPs surfaces through biotin-avidin interactions. To verify that the $KGdF_4:Tb^{3+}$ NPs were functionalized with aptamers, UV-vis absorption spectroscopy was utilized to monitor the reaction products. As shown in Fig. 3, strong absorbance of avidin before conjugation to $KGdF_4:Tb^{3+}$ NPs was observed at 280 nm (curve a). After incubation of amine-functionalized $KGdF_4:Tb^{3+}$ NPs, the supernatant was collected by centrifugation. The absorbance of the supernatant liquor is weaker at 280 nm (curve b) because part of avidin combined with the amine-functionalized $KGdF_4:Tb^{3+}$ NPs. No strong absorbance peak was detected for $KGdF_4:Tb^{3+}$ NPs (curve d). After conjugation to the aptamer, a new absorption peak at approximately 260 nm was observed (curve c). Similarly, a new DNA absorption peak appeared at approximately 260 nm after incubation of AuNPs with cDNA, which were conjugated due to Au-S interaction (curve e and f) Therefore, these results demonstrate that both aptamer-$KGdF_4:Tb^{3+}$ NPs and cDNA-AuNPs complexes were successfully formed. In addition, the aptamer-$KGdF_4:Tb^{3+}$ NPs/cDNA-AuNPs complexes were characterized by TEM imaging. As shown in Fig. 3g, many AuNPs were present on the surface of the $KGdF_4:Tb^{3+}$ NPs, indicating that the AuNPs were drawn to the $KGdF_4:Tb^{3+}$ NPs surface through hybridizing between aptamers and cDNA.

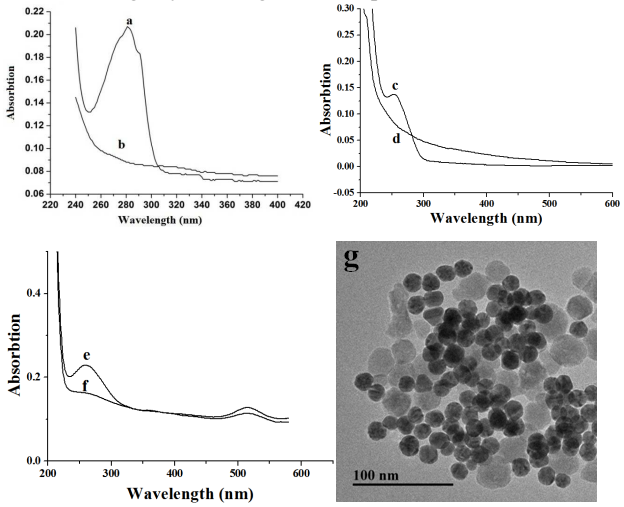

Fig. 3 Absorption spectra of an initial avidin solution (curve a) and supernatant liquor after avidin conjugation to $KGdF_4:Tb^{3+}$ NPs (b), aptamer-functionalized $KGdF_4:Tb^{3+}$ NPs (c), bare $KGdF_4:Tb^{3+}$ NPs (d), cDNA-functionalized AuNPs (e), bare AuNPs (f), and TEM image of aptamer-$KGdF_4:Tb^{3+}$ NPs/cDNA-AuNPs complexes.

Optimization of assay conditions

Several factors might affect BPA detection sensitivity in this system, such as buffer composition, pH value, incubation temperature and time. It is known that the conformation of an aptamer has a significant influence on its target affinity, which could be influenced by the ionic strength, especially Mg^{2+}. As shown in Fig. 4A, the aptamer-$KGdF_4:Tb^{3+}$ NPs/cDNA-AuNPs complexes were dissolved in buffers (25 mM Tris-HCl, 100 mM NaCl, 25 mM KCl, 5% DMSO, pH 8.0) with varied $MgCl_2$ concentrations (between 0-20 mM). Then, 5 ng·mL^{-1} of BPA was added, and the recovered fluorescence was measured after incubation for 45 min. The signal intensity was the highest in the presence of 10 mM Mg^{2+}; as a result, this concentration was chosen for all subsequent tests. The buffer pH was also optimized, as the effect of the pH corroborates the crucial role of magnesium binding to the aptamer DNA. The results of pH optimization indicated that the maximum response for 5 ng·mL^{-1} BPA occurred at pH 8.0. The incubation temperature and time also have an effect on the binding of aptamer and target. Generally, the incubation temperature is room temperature (25 °C) or 37 °C in the aptamer selection. As shown in Fig. 4C, there was no significant difference between the two temperatures. The recovered fluorescence intensity under 25 °C is a little more than that of 37 °C. Therefore, the incubation temperature was chosen at 25 °C. Fig. 4D shows the recovered fluorescence intensity of $KGdF_4:Tb^{3+}$ NPs as a function of incubation time. In the presence of the target, the curve exhibits a rapid increase in the first 20 min and reaches equilibrium over a period of 45 min, which indicates that the recognition and binding of aptamers to targets reach saturation. So, the incubation time was chosen at 45 min.

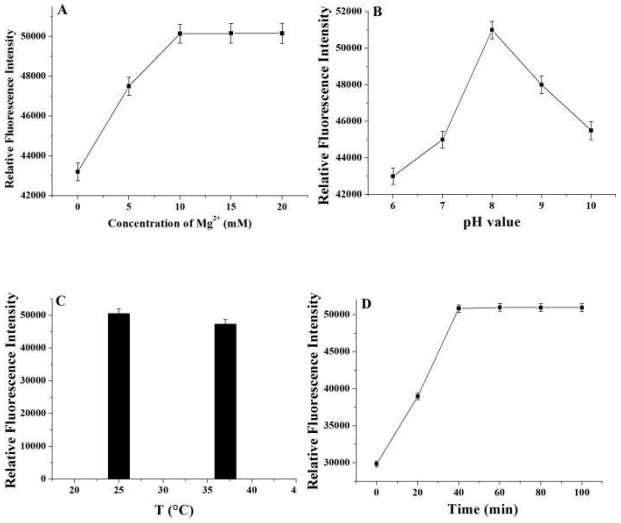

Fig.4 Effects the Mg^{2+} concentration (A), pH value (B), incubation temperature (C), and incubation time (D) on BPA detection. (BPA concentration was 5 ng·mL^{-1})

To confirm that fluorescence quenching was caused by the aptamer-$KGdF_4:Tb^{3+}$ NPs/cDNA-AuNPs complexes, several control experiments were performed. As shown in Fig. 5 (curve a), $KGdF_4:Tb^{3+}$ NPs-aptamer presented a strong fluorescence property. The strong fluorescence of aptamer-$KGdF_4:Tb^{3+}$ NPs can be almost completely quenched upon the addition of cDNA-AuNPs (curve b). In contrast, the interactions between $KGdF_4:Tb^{3+}$ NPs-aptamer and AuNPs resulted in almost no

fluorescence quenching (curve c). Aptamer-$KGdF_4$:Tb^{3+} NPs can be brought into close proximity to AuNPs surfaces through strong hybridization between aptamers and cDNA. The results indicated that the presence of aptamers and cDNA are related to the highly efficient fluorescence quenching between aptamer-$KGdF_4$:Tb^{3+} NPs and cDNA-AuNPs.

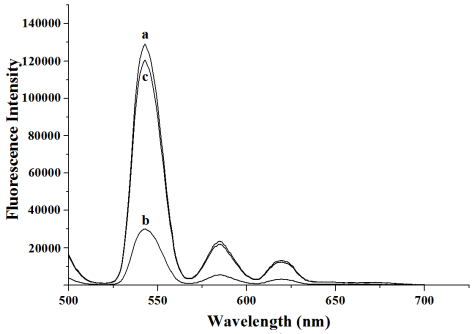

Fig. 5 Fluorescence spectra of $KGdF_4$:Tb^{3+} NPs-aptamer (a), $KGdF_4$:Tb^{3+} NPs-aptamer after incubation with AuNPs-cDNA (b), and $KGdF_4$:Tb^{3+} NPs-aptamer after incubation with AuNPs (c).

Analytical performance

As previously mentioned, in the absence of BPA, the fluorescence intensity was the minimum background fluorescence (F_0). In the presence of BPA, the aptamers preferentially bound to BPA, forming $KGdF_4$:Tb^{3+} NPs-aptamer-target complexes and thereby inducing the dehybridization of cDNA-AuNPs and fluorescence was recovered. The higher the concentration of BPA, the stronger the recovered fluorescence intensity (F) was. The fluorescence signals of $KGdF_4$:Tb^{3+} NPs-aptamer complexes at different BPA concentrations are shown in Fig. 6A. A plot of relative fluorescence intensity ($\Delta F=F-F_0$) with various BPA concentrations is shown in Fig. 6B. Under optimized conditions, linearity was obtained in the range of 0.5 ~100 ng·mL^{-1} BPA with a detection limit of 0.16 ng·mL^{-1}. The linear regression equation is described as y=430.0x+45235 (R^2=0.993). The precision expressed as the relative standard deviation (RSD) of this detection is 2.43% (obtained from a series of 7 standard samples each containing 5 ng·mL^{-1} BPA).

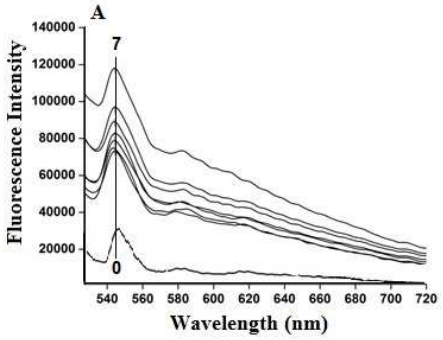

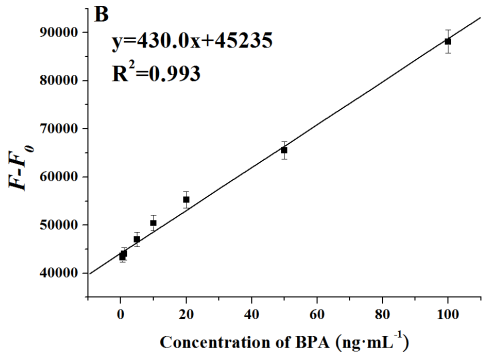

Fig. 6 Typical recording outputs for the detection of different BPA concentrations using the developed method (0~7: 0, 0.5, 1, 5, 10, 20, 50, and 100 ng·mL^{-1} BPA, respectively) (A), and standard curve of fluorescence intensity (F-F_0) versus BPA concentration (B).

Specificity evaluation and analytical application

To assess the specificity of our FRET-based aptamer biosensor for BPA detection, the influences of other BPA analogues, including phenol, acetone, propiophenone, and methylbenzene, were examined in aqueous buffer. As shown in Fig. 7, none of these analogues caused obvious changes in fluorescence, while a significant fluorescence increase was observed for BPA. These results have thus clearly demonstrated that the designed FRET-based aptamer biosensor has good specificity for BPA detection.

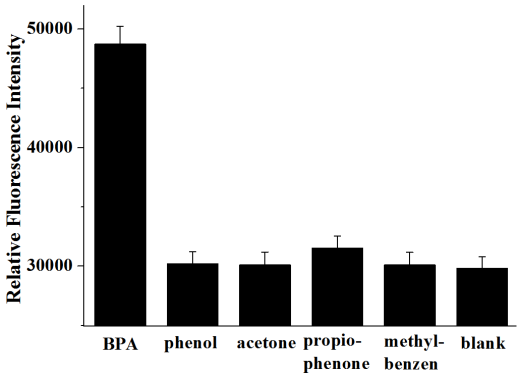

Fig. 7 Selectivity evaluation of the developed method for BPA against other analogues. (All concentrations were 5 ng·mL^{-1})

To demonstrate the extended practicality of the developed method, real mineral water samples were selected as a model platform for the detection of BPA. Five mineral water samples were spiked with BPA concentrations ranging from 0.1 to 100 ng·mL^{-1}, and then analyzed. As shown in Table 1, the results obtained by the developed method herein were in good agreement with the previous HPLC method. No significant differences were observed between the compared methods, demonstrating the feasibility of our established FRET aptamer biosensor assay. Moreover, the recoveries of BPA were between 97%~103%, indicating the high accuracy level of our developed bioassay. These analyses demonstrate that the proposed method could be applied to the analyses of BPA in real samples.

Table 1 Recovery of BPA detection in mineral water samples (n=5)

Sample	Background Content ($ng \cdot mL^{-1}$)	Added Concentration ($ng \cdot mL^{-1}$)	Detected Concentration ($ng \cdot mL^{-1}$) (mean SD)		Recovery ratio (%)
			HPLC method	developed method	
1	0	0.1	ND	ND	ND
2	0	1	ND	0.9±0.15	99
3	0	10	10±0.18	9.8±0.26	103
4	0	50	47±0.42	48±0.37	97
5	0	100	103±0.26	102±0.14	102

Conclusion

In summary, we presented a novel method for the detection of BPA based on aptamer recognition and a FRET system using $KGdF_4:Tb^{3+}$ NPs as an energy donor and AuNPs as an energy acceptor. A high quenching efficiency was easily achieved as a result of $KGdF_4:Tb^{3+}$ NPs-aptamer and AuNPs-cDNA hybridization, leading to the FRET quenching of the fluorescence of $KGdF_4:Tb^{3+}$ NPs. Moreover, the subsequent fluorescence recovery, induced by the formation of $KGdF_4:Tb^{3+}$ NPs-aptamer-BPA complexes, forced $KGdF_4:Tb^{3+}$ NPs to be far away from the Au NPs. There are also some biosensors based on aptamer for BPA detection, such as surface-enhanced raman scattering (SERS) aptasensor [31], electrochemical aptasensor [32], colorimetric aptasensor [33] and so on. These strategies are highly sensitive and specific, but the linear ranges are relative narrow, and some require rather complicated and expensive instruments. Our FRET aptamer biosensor exhibits a broad linear scope and ultralow detection limit for BPA, thus possessing excellent performance in trace analyses. In addition, FRET is a typical homogeneous assay technique, which eliminating the separation step. Our method was successfully applied to the determination of BPA levels in real samples. Furthermore, this strategy could be developed for the sensing of other aptamer-specific contaminants, and thus has a wide range of potential applications in different fields.

Acknowledgments

This work was partialy supported by NSFC (31401575, 31401576), the S&T Supporting Project of Jiangsu Province (BE2011621), National Science and Technology Support Program of China (2012BAK08B01), BK20140155, JUSRP51309A, WZ201219, and 2012BAK08B01.

Notes and references

[a] *State Key Laboratory of Food Science and Technology, Synergetic Innovation Center of Food Safety and Nutrition, School of Food Science and Technology, Jiangnan University, Wuxi 214122, China. Fax & Tel: +86 510 85917023; E-mail: wangzp@jiangnan.edu.cn*

[b] *China Rural Technology Development Center, Beijing 100045, China*

[c] *Changzhou Maternal And Child Health Care Hosptial, Changzhou 213000, China*

1 T.A. Patterson, N.C. Twaddle, C.S. Roegge, R.J. Callicott, J.W. Fisher and D.R. Doerge, *Toxicol. Appl. Pharm*., 2013, **267**, 41-48.

2 K. Kolsek, M.S. Dolenc and J. Mavri, *Chem. Res. Toxicol*., 2013, **26**, 106-111.

3 C.A. Staples, P.B. Dorn, G.M. Klecka, S.T. O'Block and L.R. Harris, *Chemosphere*, 1998, **36**, 2149-2173.

4 C.Y. Liao and K. Kannan, *J. Agric. Food Chem*., 2013, **61**, 4655-4662.

5 L.A. Hoepner, R.M. Whyatt, A.C. Just, A.M. Calafat, F.P. Perera and A.G. Rundle, *Environ. Res.*, 2013, **122**, 38-44.

6 R. Steinmetz, N.A. Mitchner, A. Grant, D.L. Allen, R.M. Bigsby and N. Ben-Jonathan, *Endocrinology*, 1998, **139**, 2741-2747.

7 Y.B. Wetherill, C.E. Petre, K.R. Monk, A. Puga and K.E. Knudsen, *Mol. Cancer. Ther.*, 2002, **1**, 515-524.

8 B.T. Akingbemi, C.M. Sottas, A.I. Koulova, G.R. Klinefelter and M.P. Hardy, *Endocrinology*, 2004, **145**, 592-603.

9 K. Inoue, K. Kato, Y. Yoshimura, T. Makino and H. Nakazawa, *J. Chromatogr. B*, 2000, **749**, 17-23.

10 E. Herrero-Hernandez, R. Carabias-Martinez and E. Rodriguez-Gonzalo, *Anal. Chim. Acta.*, 2009, **650**, 195-201.

11 R.J. W. Meesters and H.F. Schroder, *Anal. Chem.*, 2002, **74**, 3566-3574.

12 V. Becerra and J. Odermatt, *Analyst*, 2012, **137**, 2250-2259.

13 M. Aminur Rahman, M.J.A. Shiddiky, J.S. Park and Y.B. Shim, *Biosens. Bioelectron.*, 2007, **22**, 2464-2470.

14 G.R. Marchesini, E. Meulenberg, W. Haasnoot and H. Irth, *Anal. Chim. Acta*., 2005, **528**, 37-45.

15 Z.X. Zheng, Y.L. Du, Z.H. Wang, Q.L. Feng and C.M. Wang, *Analyst*, 2013, **138**, 693-701.

16 E.L. Liu and X.L. Zhang, *Anal. Methods*, 2014, **6**, 8604-8612.

17 A.D. Ellington and J.W. Szostak, *Nature*, 1990, **346**, 818-822.

18 C. Tuerk and L. Gold, *Science*, 1990, **249**, 505-510.

19 J.A. Cruz-Aguado and G. Penner, *J. Agric. Food. Chem*., 2008, **56**, 10456-10461.

20 J.C. Cox and A.D. Ellington, *Bioorgan. Med. Chem*., 2001, **9**, 2525-2531.

21 N. Duan, S.J. Wu, X.J. Chen, Y.K. Huang and Z.P. Wang, *J. Agr. Food Chem*., 2012, **60**, 4034-4038.

22 M. Szymanski, J. Noble, A. Knight, R. Porter and G. Worsley, *Anal. Methods*, 2013, **5**, 187-191.

23 G.Z. Zhu, M. Ye, M.J. Donovan, E. Song, Z.L. Zhao and W.H. Tan, *Chem. Commun.*, 2012, **48**, 10472-10480.

24 E.A. Jares-Erijman and T.M. Jovin, *Nat Biotechnol*., 2003, **21**, 1387-1395.

25 K.E. Sapsford, L. Berti and I.L. Medintz, *Angew. Chem. Int. Ed*., 2006, **45**, 4562-4588

26 M. Jo, J.Y. Ahn, J. Lee, S. Lee, S.W. Hong, J.W. Yoo, J. Kang, P. Dua, D.K. Lee, S. Hong and S. Kim, *Oligonucleotides*, 2011, **21**, 85-91.

27 X.H. Ji, X.N. Song, J. Li, Y.B. Bai, W.S. Yang and X.G. Peng, *J. Am. Chem. Soc.*, 2007, **129**, 13939-13948.

28 Z. Q. Ye, M.Q. Tan, G. Wang and J.L. Yuan, *Anal. Chem*., 2004, **76**, 513-518.

29 R. Elghanian, J.J. Storhoff, R.C. Mucic, R.L. Letsinger and C.A. Mirkin, *Science*, 1997, **277**, 1078-1081.

30. Y.P. Du, Y.W. Zhang, L.D. Sun, C.H. Yan, *Dalton T*., 2009, **40**, 8574-8581.

31. 1. H.L. Marks, M.V. Pishko, G.W. Jackson, G.L. Cote, *Anal. Chem*., 2014, **86**, 11614-11619.

32. L. Zhou, J.P. Wang, D.J. Li, Y.B. Li, *Food Chem*., 2014, **162**, 34-40.

33. Z.L. Mei, H.Q. Chu, W. Chen, F. Xue, J. Liu, H.N. Xu, R. Zhang, L. Zheng, *Biosens. Bioelectron.*, 2013, **1**, 26-30.